

Relationship Between TOA Albedo and Cloud Optical Depth as Deduced from Models and Collocated AVHRR and ERBE Satellite Observations

F.-L. Chang and Z. Li
Canada Centre for Remote Sensing
Ottawa, Ontario, Canada

S. A. Ackerman
Department of Atmospheric and Oceanic Sciences
University of Wisconsin-Madison

Introduction

It has long been recognized that clouds have a large influence on the earth's radiation budget and climate. Current cloud and radiation research programs, such as the Clouds and Earth's Radiant Energy System (CERES) and the Atmospheric Radiation Measurement (ARM) Program, play important roles in obtaining an accurate knowledge of clouds and radiation and their interactions. The study of the relationship between radiative fluxes and cloud properties can provide insight into the problem of how clouds interact with the radiation. While such a relationship has been studied extensively by means of radiative transfer modeling, little has been done using observational data. Comparison of the relationship derived from models and observations is also instrumental in understanding the fundamentals of radiative transfer within clouds.

In this study, coincident and collocated satellite observations taken from the Earth Radiation Budget Experiment (ERBE) and Advanced Very High Resolution Radiometer (AVHRR) are analyzed to investigate the relationship between the top-of-the-atmosphere (TOA) albedo and cloud optical properties for regions that are completely overcast by single-layered, low-level, and marine boundary layer clouds. The TOA albedo for overcast regions is derived from the reflected solar flux observed by ERBE at the TOA. Cloud optical depth, droplet effective radius, and cloud height are retrieved from AVHRR radiance measurements. The relationship between the TOA albedo and cloud optical properties is obtained at various solar zenith angles and locations over the oceans. Such a relationship is also compared to that obtained based on the radiative transfer model calculations.

ERBE and AVHRR Data

The ERBE and AVHRR data used in this study were obtained from the *NOAA-9* and *NOAA-10* polar orbiting satellites and were contained in the ERBE V-5 scene identification validation data. The ERBE and AVHRR observations were collected for approximately 10-minute orbital segments over two V-5 regions: the southeastern Pacific Ocean (5°S to 35°S, 80°W to 110°W) and north Atlantic Ocean (15°N to 45°N, 30°W to 60°W). The observations were taken from passes during April and July 1985 through 1988 and sampled every 5 to 6 days (see Table 1). The ERBE and AVHRR instruments are both on board the polar orbiting satellite and scan the earth in a cross-track direction, which allows for coincident observation. The spatial resolution at nadir is approximately 40 km for the ERBE radiometer. While the original resolution of the AVHRR imager is 1.1 km at nadir, data used here have a reduced resolution of 4 km, which are often referred to as the Global Area Coverage (GAC) data. It is worth noting that the ERBE and AVHRR data used in this study are constrained to only near-nadir ($< 30^\circ$) satellite zenith angles in order to limit the uncertainties caused by the angular dependence at large view angles. The ERBE scanning SW radiometer did not directly measure TOA reflected fluxes, but TOA reflected radiances. The former were estimated from the latter by means of angular correction (Smith et al. 1986). The angular correction is a major source of the uncertainty in the instantaneous ERBE flux data (Wielicki et al. 1995). Nevertheless, ERBE data have been demonstrated to be most useful for addressing some critical issues concerning clouds and the earth's radiation budget (Ramanathan et al. 1989).

Table 1. Time, locations, and satellites. Each month contains approximately 6 days (5 days apart) of data.

	Southeastern Pacific (5°S-35°S, 80°W-110°W)	North Atlantic (15°N-45°N, 30°W-60°W)
NOAA-9	04/85, 07/85, 04/86, 07/86	07/85, 07/86
NOAA-10	07/87, 07/88	07/87, 07/88

The AVHRR imager is a multichannel detector, which measures radiances at five spectral channels centered at 0.63 (0.56- 0.68) μm , 0.89 (0.72-0.98) μm , 3.7 (3.55-3.93) μm , 11 (10.3- 11.3) μm , and 12 (11.5-12.5) μm . These five channels are atmospheric window channels where gaseous absorption is weak. In this study, the radiances measured at 0.63 μm , 3.7 μm , and 11 μm were used to retrieve cloud optical depth, droplet size, and cloud top height. To study the relationship between cloud properties derived from AVHRR and radiative fluxes measured by ERBE, AVHRR GAC pixels need to be collocated within the ERBE field of view (FOV). The collocation is described in Ackerman and Inoue (1994).

Methodology

Identification of Overcast FOVs

In order to compare ERBE-observed TOA reflected fluxes with models, data analyses are performed on the spatial scale of the grid size of an ERBE FOV (~40 km). The comparisons are made for ERBE FOVs that are identified as being completely overcast with single-layered, low-level clouds (marine stratus and stratocumulus). The identification of such an overcast FOV is determined by applying the spatial coherence method (Coakley and Bretherton, 1982) to the AVHRR GAC pixels to examine the spatial uniformity of the 11- μm radiance field. For each of the ERBE FOV, which is overcast covered by a single-layered low-level cloud, the method ensures that all the GAC pixels falling within the ERBE FOV have a similar 11- μm brightness temperature (variation range $< 1^\circ \text{K}$) and the temperatures of all pixels are greater than 273° K. To further ensure that data under study are overcast, the ERBE pixels are eliminated if they contain any GAC pixels having cloud optical depth less than 2.

Retrieval of Cloud Properties

Cloud optical depth, droplet effective radius, and cloud top temperature are retrieved from AVHRR radiances observed at 0.63 μm , 3.7 μm , and 11 μm using an iterative retrieval

scheme developed by Chang (1997). The scheme compares AVHRR radiance observations with look-up tables of radiative transfer calculations at 0.63 μm , 3.7 μm , and 11 μm channels and iterates the retrieval process at each of the three channels (i.e., retrieving cloud optical depth at 0.63 μm , retrieving droplet effective radius at 3.7 μm , and retrieving cloud top temperature at 11 μm). During the iterations, new retrieved cloud properties are used and the iteration stops when the new retrieved cloud optical depth, droplet effective radius, and cloud top temperature all converge to stable values.

The look-up tables cover the range of the radiances that would be observed by an AVHRR imager and include components of radiances reflected, emitted, and transmitted by clouds and the atmosphere and radiances reflected and emitted by sea surface. The radiative transfer calculations are made for a variety of cloud optical depths, droplet effective radii, cloud top heights, and satellite-earth-sun viewing geometries. The adding-doubling method is used to solve the radiative transfer equation. Cloud droplets are assumed to be water sphere with a gamma size distribution. Mie theory is used to compute the optical properties of water droplets. Correlated- k models developed for the AVHRR channels by Kratz (1995) are used to determine the atmospheric absorption. The profiles of the atmospheric temperature, humidity, and ozone are derived by interpolation from the McClatchey (1972) standard atmospheric models for the midlatitude summer, midlatitude winter, and tropics. The interpolation process is according to the differences in the sea surface temperature between local observation and models. The sea surface is assumed to be Lambertian with albedos varying with wavelength (0.03 for 0.63 μm and 0.01 for 3.7 μm). The maritime aerosol optical properties are adopted from the LOWTRAN-7 model with an optical depth of 0.1.

Computation of the Broadband TOA Fluxes

The retrieved cloud optical depths and droplet effective radii are employed to compute the reflected solar fluxes at the TOA using a broadband radiative transfer model of Masuda and Takashima (1986). Like that in Chang (1997), the model also employs an adding-doubling routine, except that it calculates the broadband fluxes with 120 wavelength bands (various band widths) spanning 0.2 μm to 25 μm . For the flux calculations, the spectral solar constant is obtained from Thekaekara (1974). The cloud layer is placed at fixed altitudes between 0.5 km to 1.5 km. This approximation is close to those observed cloud top altitudes for the single-layered, low-level systems. Besides, LOWTRAN-7 model is used to calculate the atmospheric transmittance at

120 wavelengths. The comparison between Kratz's correlated- k models and LOWTRAN-7 shows good agreement in the transmittance for the spectral ranges of $0.56\ \mu\text{m}$ to $0.68\ \mu\text{m}$ and $3.55\ \mu\text{m}$ to $3.93\ \mu\text{m}$. The other properties, such as the atmosphere, sea surface, and aerosol, are treated the same as in the Chang model.

Figure 1 shows the TOA reflected fluxes computed by the Masuda and Takashima model and those observed by ERBE for the overcast FOVs. In the model computation, the flux corresponding to an ERBE overcast pixel is obtained by averaging the fluxes computed for all of the GAC pixels falling within the FOV of the ERBE pixel. The linear least-squares fits are also plotted for the data obtained in each month and region. The slopes of the least-squares fits range between 0.58-0.84. Figure 2 shows the difference in the TOA albedo between model computation and ERBE observation for the data shown in Figure 1. The differences are plotted as functions of cloud optical depth, droplet effective radius, and solar zenith angle. The figure shows that the differences between modeled and observed albedos (model - observation) decrease from positive to negative values as cloud optical depth increases. The dependence of the difference on either the droplet effective radius or solar zenith angle is very weak.

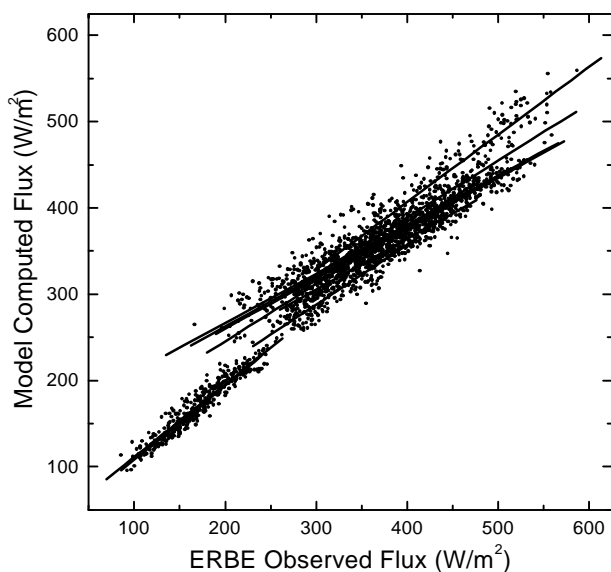


Figure 1. ERBE observed and model computed TOA reflected fluxes (W/m^2) for overcast FOVs. The lines are the least-squares fit to data of different month and location.

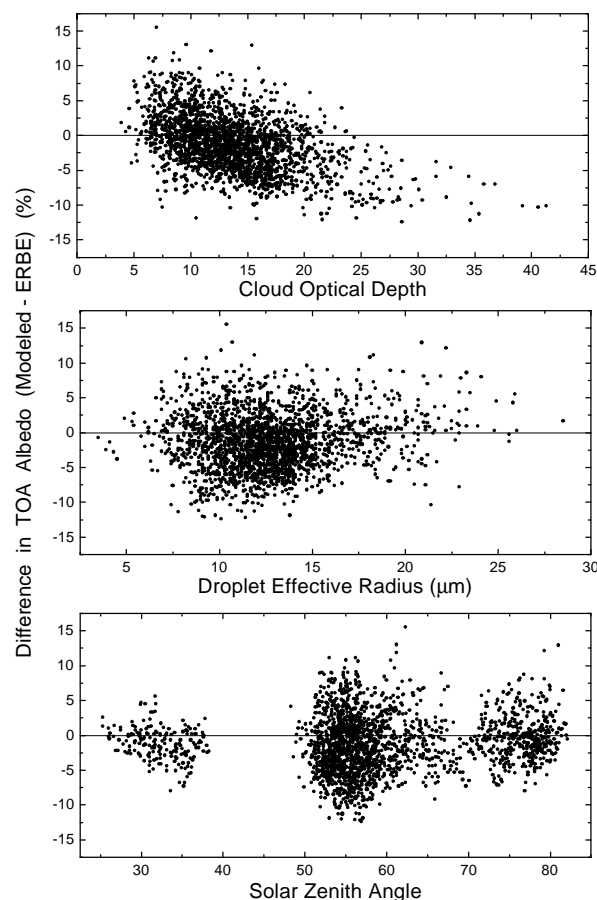


Figure 2. Difference (%) between model computed and ERBE observed TOA albedos as functions of cloud optical depth, droplet effective radius, and solar zenith angle.

Relationship between TOA Albedo and Cloud Optical Depth

The relationship between the TOA albedo and cloud optical depth is investigated for both model computation and ERBE observation. Figure 3 shows such a relationship for the data obtained in four different months in 1985-1988 with various solar zenith angles and locations. The dots are the ERBE observations from overcast FOVs, while the lines show model computations with dashed lines indicating the uncertainties due to a change of factor 2 in the column amount of water vapor, ozone, aerosol, and trace gases and in the surface reflectance and cloud altitude and a change of $\pm 4\ \mu\text{m}$ in droplet effective radius. The solar zenith angle given in each figure is the monthly mean and the actual range is approximately $\pm 5^\circ$ from the mean.

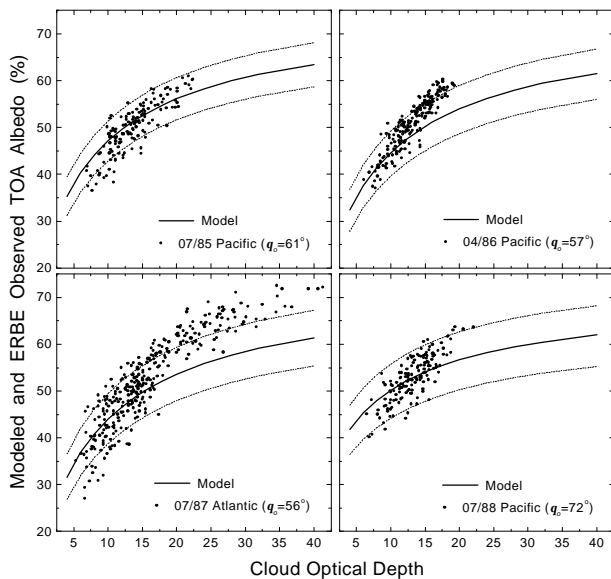


Figure 3. TOA albedos (%) from ERBE observations and model computations. Dashed lines indicate the uncertainties of model computations, which are described in the text.

As illustrated in Figure 3, positive and negative biases exist for all the subsets of the data. The observed albedos are generally smaller than the model computations when cloud optical depth is small ($< \sim 15$) and are generally larger when cloud optical depth is large ($> \sim 20$). It appears that the increasing rate in TOA albedo with increasing cloud optical depth from ERBE observations is drastically more rapid than that from model computations. Such a dramatic discrepancy in TOA albedo between model and observation may be larger than 10% for large cloud optical depth. The discrepancy is attributable to either that the TOA fluxes from ERBE are overestimated and/or the cloud optical depths from AVHRR retrievals are underestimated.

Assuming that the ERBE data are free of uncertainty, cloud optical depths were also retrieved from ERBE broadband fluxes, which are compared to those retrieved from AVHRR radiances. The comparison is shown in Figure 4. The difference (AVHRR cloud optical depth minus ERBE cloud optical depth) is plotted as a function of AVHRR cloud optical depth. The ERBE cloud optical depths are retrieved by comparing each of the ERBE fluxes to a look-up table of TOA fluxes computed using the Masuda and Takashima model for a variety of cloud optical depths, droplet effective radii, and solar zenith angles. For specific solar zenith angle and using the droplet effective radius retrieved from AVHRR, ERBE cloud optical depth is retrieved by interpolation from the look-up tables. Figure 4 shows

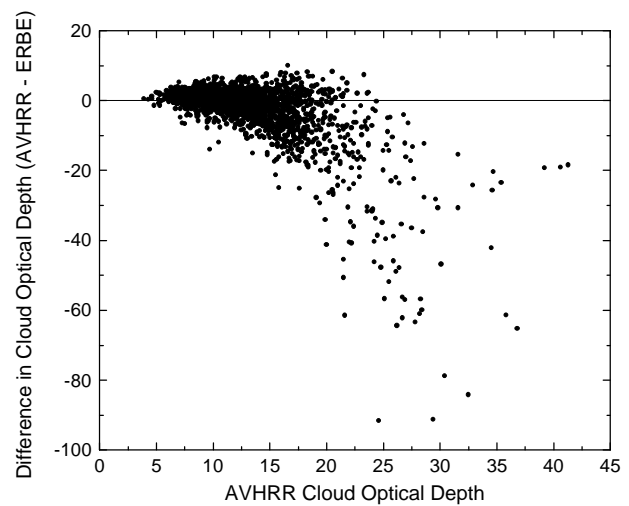


Figure 4. Absolute difference in cloud optical depth between AVHRR and ERBE retrievals.

that the cloud optical depths retrieved from AVHRR are systematically smaller than those inferred from ERBE retrievals. The underestimates are as large as a factor of 2-4 for cloud optical depth > 20 .

Conclusions

The relationship between radiative fluxes and cloud properties is the core between cloud and radiation interaction. Based on the coincident and collocated satellite data from ERBE and AVHRR, the relationship between TOA albedo and cloud optical depth is derived from both satellite observation and model computation for regions that are completely overcast by a single-layered, low-level system, a typical form of the marine stratus and stratocumulus. While using only data with satellite zenith angles $< 30^\circ$, it is found that ERBE TOA albedos tend to be lower than model computations for small cloud optical depth ($< \sim 15$) and higher for large cloud optical depth ($> \sim 20$). The absolute difference in the albedo reaches more than 10% for large cloud optical depths. The finding suggests that the ERBE TOA albedos increase with increasing cloud optical depth at a much faster rate than the model predicts. The magnitude of the discrepancy cannot be explained by the uncertainties in model input parameters such as atmospheric constituents, cloud height, surface properties, and droplet effective radius.

The discrepancy could result from an overestimate in the ERBE fluxes due to scene misidentification and/or an incorrect angular dependence model (Ye and Coakley 1996). As far as the data used in this study, more than 95%

of the FOVs that are identified as being completely overcast are in fact identified as being only most cloudy by ERBE. Another possible explanation for the discrepancy is the incorrect retrievals of cloud optical depth due to the erroneous calibration of the AVHRR radiances. The plane-parallel assumption employed in the radiative transfer calculations may also contribute to the discrepancy. Further research is needed to unravel the discrepancy.

Acknowledgments

This work was supported by a Natural Sciences and Engineering Research Council (NSERC) of Canada, Visiting Fellowship awarded to FLC and research grants to Z. Li from U.S. Department of Energy Grant No. DE-FG02-97ER62361.

References

- Ackerman, S. A., and T. Inoue, 1994: Radiation Energy Budget studies using collocated AVHRR and ERBE observations. *J. Appl. Meteorol.*, **33**, 370-378.
- Chang, F.-L., 1997: Properties of low-level marine clouds as deduced from AVHRR satellite observations. Ph.D. Dissertation, Oregon State University, 335 pp.
- Coakley, J. A., Jr., and F. P. Bretherton, 1982: Cloud cover from high-resolution scanner data: Detecting and allowing for partially filled fields of view. *J. Geophys. Res.*, **87**, 4917-4932.
- Kratz, D. P., 1995: The correlated k -distribution technique as applied to the AVHRR channels. *J. Quant. Spectrosc. Radiat. Transfer*, **53**, 501-517.
- Masuda, K., and T. Takashima, 1986: Computational accuracy of radiation emerging from the ocean surface in the model atmosphere-ocean system. *Pap. Meteorol. Geophys.*, **37**, 1-13.
- McClatchey, R. A., R. W. Fenn, J. E. Selby, F. E. Volz, and J. S. Garing, 1972: *Optical Properties of the Atmosphere*. Air Force Cambridge Research Laboratories. AFCRL-72-0497, No. 411, 108 pp.
- Ramanathan, V., et al. 1989: Cloud-radiative forcing and climate: Results from the Earth Radiation Budget Experiment. *Science*, **243**, 57-63.
- Smith, G. L., R. N. Green, E. Raschke, L. M. Avis, J. T. Suttles, B. A. Wielicki, and R. Davies, 1986: Inversion methods for satellite studies of the earth's radiation budget: Development of algorithms for the ERBE mission. *Rev. Geophys.*, **24**, 407-421.
- Thekaekara, M. P., 1974: Extraterrestrial solar spectrum, 3000-6100Å at 1-Å intervals. *Appl. Opt.*, **13**, 518-522.
- Wielicki, B. A., R. D. Cess, M. D. King, D. A. Randall, and E. F. Harrison, 1995: Mission to Planet Earth: Role of clouds and radiation in climate. *Bull. Amer. Meteorol. Soc.*, **76**, 2125-2153.
- Ye, Q., and J. A. Coakley, Jr., 1996: Biases in earth radiation budget observations, Part II: Consistent scene identification and anisotropic factors. *J. Geophys. Res.*, **101**, 21,253-21,263.